Closer Proximity between Opposing Domains of Vertebrate Calmodulin Following Deletion of Met^{145}-Lys^{148}†

Dan Yin, Hongye Sun, Deborah A. Ferrington, and Thomas C. Squier*

Biochemistry and Biophysics Section, Department of Molecular Biosciences, University of Kansas, Lawrence, Kansas 66045-2106

Received April 25, 2000

ABSTRACT: To investigate the structural linkage between the opposing globular domains in vertebrate calmodulin (CaM), we have constructed a CaM mutant (CaMX^{145}) deficient in the last four amino acids between Met^{145} and Lys^{148} at the carboxyl terminal. Circular dichroism and fluorescence spectroscopic measurements were used to detect changes in the average secondary and tertiary structure of CaMX^{145} in comparison to full-length CaM. Complementary measurements of the maximal calcium-binding stoichiometry and ability to activate the plasma membrane (PM) Ca−ATPase permit an assessment of the functional significance of observed structural changes. In comparison with native CaM, we find that CaMX^{145} exhibits (i) a large reduction in α-helical content, (ii) a dramatic decrease in the average spatial separation between the opposing globular domains, (iii) the loss of one high-affinity calcium-binding site, and (iv) a diminished binding affinity for the PM−Ca−ATPase. Thus, the sequence near the carboxyl terminus functions to stabilize high-affinity calcium binding at one site and facilitates important intramolecular interactions that maintain CaM in an extended conformation. However, despite the large conformational changes resulting from deletion of the last four amino acids at the carboxyl terminal, CaMX^{145} can fully activate the PM−Ca−ATPase. These results indicate that target protein binding can restore the nativelike structure critical to function, emphasizing that the structure of the central helix is not critical to CaM function under equilibrium conditions. Rather, the central helix functions to maintain the spatial separation between the opposing domains in CaM that may be critical to high-affinity binding and the rapid activation of the PM−Ca−ATPase, which are necessary for optimal calcium signaling. Thus, following initial association between CaM and target proteins, structural changes involving the carboxyl-terminal sequence have the potential to play an important role in triggering the structural collapse of CaM that facilitates the rapid and cooperative binding of the opposing globular domains with target proteins, which is important to high-affinity binding and rapid enzyme activation.

Calmodulin (CaM) plays a key role in cellular regulation by virtue of its calcium-dependent activation of numerous target proteins, including the plasma membrane (PM) Ca−ATPase involved in the maintenance of the calcium gradient necessary for intracellular signaling (*1*). CaM contains two globular domains separated by an extended central helix located between Glu^{67} and Phe^{92} (Figure 1) (*2*). Calcium-binding functions to alter interhelical angles between α-helical elements within each globular domain, resulting in the exposure of hydrophobic-binding sites that mediate CaM binding to a range of different target proteins (*3*−*5*). At physiological ionic strengths, the central helix adopts conformationally distinct structures in apo- and calcium-saturated CaM that function to alter the Stokes radius (*6, 7*). Under these conditions the opposing globular domains are structurally coupled, and intermediate conformations associated with partial calcium occupancy have been observed (*6, 8, 9*). Upon-binding target proteins the central helix becomes conformationally disordered, permitting the two globular domains to bind to CaM-binding sequences in a diverse array of target proteins with variable recognition sequences (*10*−*12*). The structural coupling between the opposing globular domains of CaM is disrupted at low ionic strength (*7*). Thus, small changes in specific molecular interactions that normally stabilize the central helix may function as a molecular switch that has the potential to promote the ordered binding of CaM to target proteins (*7, 13*−*17*). It is, therefore, of interest to identify the intramolecular interactions within CaM that modulate the stability of the central helix and define the spatial separation between the opposing globular domains in CaM. In this respect, it is interesting that substantial interdomain interactions have been observed in both vertebrate and yeast CaM that function to reduce the calcium affinity of CaM, which are modulated by the sequence near the carboxyl terminus (*9, 18, 19*). Since the fourth high-affinity calcium-binding site is absent in yeast CaM (Table 1), the enhanced structural interactions between the opposing domains may, in part, be the result of differences in interhelical contact interactions that normally function to stabilize calcium-activated CaM in the open form and which modulate interdomain interactions (*5*). Consistent with this interpretation, elimination of calcium-binding site 4 by site-directed mutagenesis enhances the structural coupling between the opposing globular domains in *Drosophila* CaM (*20, 21*). These structural differences are of interest since (i) yeast CaM, (ii) mutant *Drosophila* CaM following

† Supported by the National Institute of Health Grants AG12993 and AG17996.

* To whom correspondence should be addressed. Tel.: (785)864-4008. Fax: (785)864-5321. E-mail: tsquier@ukans.edu.

10.1021/bi000949y CCC: $19.00
Published on Web 07/27/2000

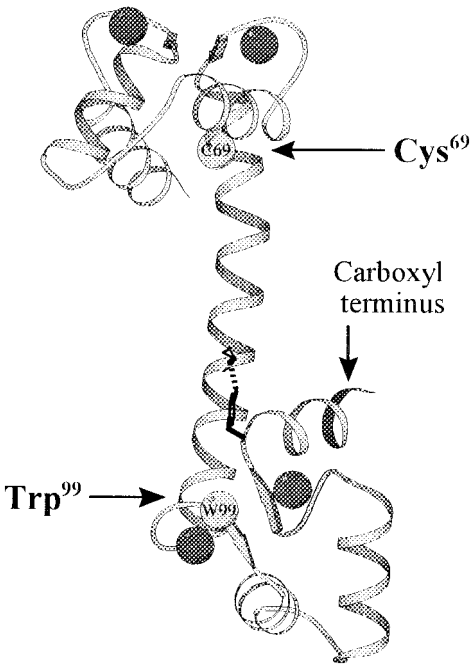

FIGURE 1: Ribbon drawing depicting the backbone fold of calcium-saturated CaM. The relative positions of Cys^{69} and Trp^{99} (light gray spheres) are indicated relative to the four high-affinity calcium-binding sites (black spheres). Ribbons represent the protein backbone of CaM, while arrows represent antiparallel β-sheet elements. The side chains of Glu^{82} and Tyr^{138} and the associated hydrogen bond between these amino acids are illustrated. Coordinates are taken from Brookhaven Protein Data Bank file 1cll (*29*). Illustration was created using MolScript *(75*).

elimination of calcium-binding site 4, and (iii) vertebrate CaM following oxidative modification of a methionine located near the carboxyl terminal (i.e., Met^{144} or Met^{145}) exhibit alterations in the conformational coupling between the opposing domains and often function as poor activators of CaM-dependent vertebrate enzymes, including the PM−Ca−ATPase (*22*−*28*). These results suggest that the structural coupling between the opposing globular domains in calcium-activated CaM is modulated by the conformation near the carboxyl terminal, which may be functionally important. Therefore, to explore the possible role of structural interactions involving the sequence near the carboxyl terminal α-helix in modulating interdomain interactions in CaM, we have used site-directed mutagenesis to delete the last four amino acids (i.e., Met^{145}-Thr^{146}-Ala^{147}-Lys^{148}) in the carboxyl terminal domain through substitution of a stop codon in place of codon encoding Met^{145}. These amino acids are highly variable among different CaM isoforms (Table 1), and the side-chain and main-chain atoms associated with the four residues at the carboxyl terminal have the largest temperature factors in the crystal structures of calcium-activated CaM (*2*, *29*). Furthermore, while Met^{145} is conserved among different CaM sequences, it is not involved in the activation of the PM−Ca−ATPase (*30*). Thus, the major effect of removing the carboxyl-terminal four amino acids is expected to involve the destabilization of the carboxyl-terminal α-helix, located between Tyr^{138} and Thr^{146} (*2*), which has the potential to alter helical interactions within the carboxyl-terminal domain and disrupt important intramolecular interactions critical to the structural coupling between the opposing globular domains that may involve, for example, the four-helix bundle in the carboxyl-terminal domain and the hydrogen bond between Tyr^{138} and Glu^{82} (Figure 1) (*2*, *5*, *26*, *31*).

To identify the effect of deleting the last four amino acids at the carboxyl terminal on the structure of CaM, we have used circular dichroism (CD) and fluorescence spectroscopy to identify alterations in the secondary and tertiary structure of CaM. To measure possible conformational changes of the central helix, Leu^{69} and Tyr^{99} were respectively substituted with Cys and Trp (Figure 1). Side chains of Leu^{69} and Tyr^{99} residues are not involved in target recognition, and this mutant CaM has previously been shown to fully activate the PM−Ca−ATPase (*7*). Therefore, when fluorescence resonance energy transfer (FRET) is used, the spatial separation can be measured between Trp^{99} and a suitable chromophore (i.e., AEDANS) bound to Cys^{69}. We report that deletion of Met^{145}-Lys^{148} results in (i) a large decrease in α-helical content, (ii) a substantial decrease in the spatial separation between Trp^{99} and AEDANS bound to Cys^{69}, and (iii) the loss of one high-affinity calcium-binding site, suggesting that the structure that is normally assumed upon calcium binding to site 4 is critical in maintaining calcium-activated CaM in an extended conformation. However, while these structural changes decrease the affinity between CaM and the PM−Ca−ATPase, deletion of Met^{145}-Lys^{148} has no effect on the maximal CaM-dependent activation of the PM−Ca−ATPase. These later results are consistent with earlier examples in which target protein binding has been shown to restore native-like structural interactions necessary for enzyme activation (*32*−*34*).

EXPERIMENTAL PROCEDURES

Materials. HEPES (*N*-[2-hydroxyethylpiperazine-*N*′-[2-ethansulfonic acid]) and TRIS free base (tris[hydroxymethyl]-aminomethane) were purchased from Research Organics Inc. (Cleveland, OH). Chelix 100 was obtained from Sigma (St. Louis, MO). 1,5-IAEDANS [5-((((2-iodoacetyl)amino)ethyl)-amino)naphthalene-1-sulfonic acid] was obtained from Molecular Probes, Inc. (Eugene, OR). T4 DNA ligase and T4 DNA polymerase were obtained from Promega (Madison, WI). 5′-Phosphorylated complementary oligonucleotides used for site-directed mutagenesis were obtained from Macromolecular Resources (Colorado State University, Ft. Collins, CO). Phenyl-Sepharose CL-4B was obtained from Pharmacia (Piscataway, NJ). A micro BCA protein assay reagent kit was obtained from Pierce (Rockford, IL). cDNA encoding chicken CaM was subcloned into the expression vector pALTER-Ex1 (Promega, Madison, WI), overexpressed in *E. coli* strain JM109(DE3) (Promega, Madison, WI), and purified essentially as previously described using phenyl Sepharose CL-4B and weak anion exchange HPLC (*35*, *36*). Site-directed substitutions of $Tyr^{99} \rightarrow Trp^{99}$ and $Leu^{69} \rightarrow Cys^{69}$, the insertion of a stop codon, and chemical derivatization of Cys^{69} with IAEDANS were done as previously described (*7*). Masses of purified CaM and CaM mutants were confirmed by ESI-MS, as previously described (*26*). Erythrocyte ghost membranes containing the PM−Ca−ATPase were purified from porcine blood, essentially as previously described (*37*). Purified CaM and erythrocyte ghost membranes were stored at −70 °C.

Table 1: Comparison of Carboxyl-Terminal Amino Acid Sequences for CaM Isoforms[a]

Species	121	148
Homo sapiens (human)	VDEMI READ I DGDGQVNYEEFVQMMTAK	
Bos taurus (cow)		
Drosophila melanogaster (fruit fly)	----------T---S-	
Stichopus japonicus (sea cucumber)		
Renilla reniformis (sea pansy)	----------K---S-	
Metridium senile (sea anemone)	----------K---S-	
Triticum aestivum (wheat)		
Spinacia oleracea (spinach)	---------V-----I-------KV-M--	
Daucus carota (carrot)		
Solanum tuberosum L. (potato)	---------V-----I--D---KV-M--	
Leaf mustard	-----K---V-----I-------KV-M--	
Caenorhabditis elegans	----------T---T-	
Ciona intestinalis	---------V----------N---N-	
Macrocystis pyrifera	----------I-------K--M--	
Phytophthora infestans	----------I-------K--MS-	
Achlya klebsiana		
Dictyostelium discoideum	---------L--------D---K--IVRN	
Pleurotus cornucopiae (mushroom)	----------I-------K--LS-	
Toxoplasma gondii	---------V-----I-------K--	
Acanthamoeba	---------V--------D---K--L--	
Trypanosoma cruzi	---------V-----I-------K--MS-	
Tetrahymena pyriformis	----------HI-------R--M--	
Stylonychia lemnae	---------V----HI-------R--M--	
Saccharomyces cervisiae (yeast)	--D-L--VS*--S-EI-IQQ-AALLSK	

[a] Nonidentical amino acids in CaM isoforms are indicated, while identical residues are denoted by dashes (*73*). Underlined amino acids in vertebrate CaM correspond to calcium-binding ligands. * indicates the absence of the corresponding amino acid in the sequence of CaM from *Saccharomyces cervisiae*.

Enzymatic Assays. CaM concentration was determined by the micro BCA method, as previously described (*7*). The erythrocyte ghost membrane protein concentration was measured using the Biuret method (*38*), using BSA[1] as the standard. Rates of ATP hydrolysis for the erythrocyte PM−Ca−ATPase were determined in a solution containing approximately 16 nM Ca−ATPase (i.e., 0.4 mg/mL porcine erythrocyte ghost membranes) in buffer A [100 mM HEPES (pH 7.5), 0.1 M KCl, 5 mM $MgCl_2$, 0.1 mM EGTA, 5 mM ATP, and 4 μM A23187] at 37 °C by measuring phosphate release, as previously described (*39*). Free calcium concentrations were calculated, as previously described (*40*). To assay the CaM-dependent activation of PM−Ca−ATPase, the free calcium concentration was maintained at 30 μM to fully saturate the calcium-binding sites of the PM−Ca−ATPase. The concentration of CaM was maintained at 0.36 μM to assay the calcium-dependent activation of PM−Ca−ATPase, which fully saturates the CaM-binding sites on the PM−Ca−ATPase.

Equilibrium Dialysis. The stoichiometry of calcium binding to CaM was determined using 1.0 mM $^{45}CaCl_2$ (20 000 cpm/nmol) equilibrated with 12 μM CaM (0.2 mg/mL) using a 1-mL dialysis cell separated by a dialysis membrane with a molecular weight cutoff of 10 000 Da in a buffer containing 100 mM HEPES (pH 7.5), 0.1 M KCl, and 1 mM $MgCl_2$, essentially as previously described (*27*). Prior to equilibration, incubation with Chelix 100 resin was used to prepare apo-CaM.

Determination of Free CaM Concentrations. The concentrations of CaM free in solution were obtained from the following relationship,

$$[\mathrm{CaM}]_{\mathrm{free}} = [\mathrm{CaM}]_{\mathrm{total}} - \frac{(V - V_{\mathrm{min}})}{(V_{\mathrm{max}} - V_{\mathrm{min}})} \times [\mathrm{PMCA}]_{\mathrm{total}} \quad (1)$$

where V_{max} is the maximal calmodulin-dependent ATPase activity, V_{min} is the CaM-independent ATPase activity, V is the observed ATPase activity at a defined concentration of CaM, $[CaM]_{free}$ is the concentration of CaM free in solution,

[1] Abbreviations: BSA, bovine serum albumin; CaM, calmodulin; CD, circular dichroism; ESI-MS, electrospray ionization mass spectrometry; FRET, fluorescence resonance energy transfer; HPLC, high-performance liquid chromatography; HW, full width at half-height of a Gaussian distance distribution; 1,5-IAEDANS, 5-((((2-iodoacetyl)-amino)ethyl)amino)naphthalene-1-sulfonic acid; IPTG, isopropyl thio-β-D-galactoside; K_{sv}, Stern−Volmer quenching constant; k_q, bimolecular collisional quenching constant; NATA, *N*-acetyl-L-tryptophanamide; *P*, steady-state polarization; PMCA or PM−Ca−ATPase, erythrocyte plasma membrane Ca−ATPase; r_{app}, apparent distance between donor and acceptor chromophores; r_0, initial anisotropy at time zero; R_{av}, average distance between donor and acceptor chromophores; t_R, HPLC retention time; $\bar{\tau}$, mean fluorescence lifetime $= \Sigma\alpha_i\tau_i$; $\langle\tau\rangle$, average fluorescence lifetime $= \Sigma\alpha_i\tau_i^2/\Sigma\alpha_i\tau_i$; t_r, HPLC retention time; ϕ, rotational correlation time.

$[CaM]_{total}$ is the total concentration of CaM added to the solution, and $[PMCA]_{total}$ is the total binding capacity of the PM−Ca−ATPase in erythrocyte ghosts for CaM. The PM−Ca−ATPase is the only high-affinity CaM-binding protein in erythrocyte ghosts, which have previously been shown to bind 40 pmol of CaM per mg of protein (*25*).

Determination of Binding Affinities between CaM and the PM−Ca−ATPase. The CaM-dependent activation of the PM−Ca−ATPase by CaM was used to estimate the apparent affinities between the opposing globular domains of CaM and the CaM-binding sequence of PM−Ca−ATPase. This analysis takes into account that CaM contains two binding domains that must both associate with binding sites within the CaM-binding sequence of the PM−Ca−ATPase to enhance enzyme activity. Initial binding between CaM and target proteins, including the PM−Ca−ATPase, involves the association of the carboxyl-terminal domain (*41, 42*). Therefore, the concentration of the amino-terminal domain of CaM (i.e., CaMN) available for binding is equal to that of the carboxyl-terminal domain of CaM (CaMC) bound to the PM−Ca−ATPase (PMCA). Consideration of this binding mechanism permits one to write the following binding equilibria:

$$\text{PMCA} + \text{CaMC} \leftrightarrows \text{CaMC·PMCA}$$

$$\text{where } K_{dl} = \frac{[\text{PMCA}]_{free} \times [\text{CaMC}]_{free}}{[\text{CaMC·PMCA}]} \quad (2)$$

and

$$\text{CaMC·PMCA} + \text{CaMN} \leftrightarrows \text{CaMC·PMCA·CaMN}$$

$$\text{where } K_{d2} = \frac{[\text{CaMC·PMCA}] \times [\text{CaMN}]_{free}}{[\text{CaMC·PMCA·CaMN}]} \quad (3)$$

It should be noted that the structural linkage between the opposing globular domains in CaM implies that the effective concentration of the amino-terminal domain (i.e., $[CaMN]_{free}$) is determined by the concentration of CaM that is bound through the carboxyl-terminal domain to the PM−Ca−ATPase (i.e., [CaMC·PMCA]). For this reason, [CaMC·PMCA] = $[CaMN]_{free}$. This equality implies that K_{d2} can be rearranged to the following form:

$$K_{d2} = \frac{[\text{CaMC·PMCA}]^2}{[\text{CaMC·PMCA·CaMN}]} \quad (4)$$

Now, since activation of the PM−Ca−ATPase requires association of both domains, this implies the following relationship:

$$\frac{[\text{PMCA}]_{active}}{[\text{PMCA}]_{total}} = \frac{[\text{CaMC·PMCA·CaMN}]}{[\text{PMCA}]_{free} + [\text{CaMC·PMCA}] + [\text{CaMC·PMCA·CaMN}]} \quad (5)$$

Since [CaMC·PMCA] ≪ [CaMC·PMCA·CaMN] (*42*), the above relationship can be further simplified:

$$\frac{[\text{PMCA}]_{active}}{[\text{PMCA}]_{total}} = \frac{[\text{CaMC·PMCA·CaMN}]}{[\text{PMCA}]_{free} + [\text{CaMC·PMCA·CaMN}]} \quad (6)$$

Now, upon substitution one can express the CaM-dependent activation of the PM−Ca−ATPase in terms of known variables, taking into account that under conditions where the opposing domains of CaM are connected that $[CaM]_{free}$ equals $[CaMC]_{free}$.

$$\frac{\text{PMCA}_{active}}{\text{PMCA}_{total}} = \frac{\dfrac{[\text{PMCA}]_{free} \times [\text{CaM}]_{free}^{\,2}}{K_{dl}^{\,2} \times K_{d2}}}{1 + \dfrac{[\text{PMCA}]_{free} \times [\text{CaM}]_{free}^{\,2}}{K_{dl}^{\,2} \times K_{d2}}} \quad (7)$$

The concentration of unbound PMCA (i.e., $[PMCA]_{free}$) can be expressed in terms of [CaMC], K_{d1}, K_{d2}, and $[PMCA]_{total}$ upon further substitution and a consideration of the conservation of mass, where

$$[\text{PMCA}]_{free} = -1 + \frac{\left(1 + 4 \times \dfrac{[\text{CaM}]_{free}^{\,2} \times [\text{PMCA}]_{total}}{K_{1d}^{\,2} \times K_{2d}}\right)^{1/2}}{\dfrac{2 \times [\text{CaM}]_{free}^{\,2}}{K_{1d}^{\,2} \times K_{2d}}} \quad (8)$$

The calmodulin-dependent activation of the PM−Ca−ATPase can therefore be fit to eq 7, which takes into account the sequential and ordered binding mechanism of CaM with the Ca−ATPase (*42*). In this equation, $[CaM]_{free}$ is the concentration of CaM not bound to the PM−Ca−ATPase. $[PMCA]_{total}$ and $[PMCA]_{free}$ respectively represent the total concentration of the PM−Ca−ATPase and the concentration of the Ca−ATPase with no CaM bound. K_{1d} corresponds to the dissociation constant for binding of the carboxyl-terminal domain of CaM to the Ca−ATPase and K_{2d} is the apparent dissociation constant for the amino-terminal domain of CaM, ignoring the large increase in the effective concentration of the amino-terminal domain resulting from the initial association of the carboxyl-terminal domain to the Ca−ATPase (*7*, *42*).

Calculation of Apparent Calcium Affinities. The relative affinities and possible cooperative interactions between individual calcium-binding sites were assessed by fitting the data to the following equation:

$$Y = \left[A \times \left[\frac{Y_{max} \times [Ca^{2+}]^{n_1}}{k_{dl}^{\,n_1} + [Ca^{2+}]^{n_1}}\right] + (1 - A) \times \left[\frac{Y_{max} \times [Ca^{2+}]^{n_2}}{k_{d2}^{\,n_2} + [Ca^{2+}]^{n_2}}\right]\right] \times Y_{max} + \text{minimum} \quad (9)$$

Y equals the calcium-dependent response, which is equal to either the calcium-dependent ATPase activity (Figure 4A) or calcium-dependent changes in the fluorescence quantum yield of Trp^{99} (Figure 6C). Y_{max} is the maximal change in the ATPase activity or fluorescence signal, k_{d1} and k_{d2} are the apparent calcium dissociation constants, n_1 and n_2 are coefficients that are related to the cooperativity of enzyme activation or the fluorescence response, and *A* is an amplitude weighting factor. When $A = 1$, eq 9 reduces to the Hill

equation. We emphasize that calcium-dependent changes in the fluorescence response of Trp^{99} are not expected to be linear with respect to calcium binding, and as a result there is no precise relationship between the absolute value of *n* and the number of ligand-binding sites.

Circular Dichroism Spectroscopy. Circular dichroism (CD) spectra were measured at 25 °C using a Jasco J-710 spectropolarimeter (Jasco Corporation, Tokyo, Japan) and a temperature-jacketed spectral cell with a path length of 10 cm. The apparent α-helical content was determined using the program Contin, as previously described (*43*).

Fluorescence Measurements. Steady-state or frequency-domain lifetime and anisotropy measurements involved either the 333-nm output from a Coherent Innova 400 argon ion laser (Santa Clara, CA) to excite AEDANS labeled at Cys^{69} or the tripled output (297 nm) of a Ti:sapphire laser (Coherent, Mira 900) tuned to 891 nm, whose frequency was reduced to 5 MHz using a Coherent pulse picker (model 9200), to excite Trp^{99}, as previously described (*7*). The emitted fluorescence intensity was respectively detected after a monochromator centered at 346 nm (8 nm band-pass) or a Schott long-pass GG400 filter. Samples contained 6 μM CaM in buffer B [0.1 M HEPES (pH 7.5), 0.1 M KCl, and 0.1 mM EGTA] in the absence and presence of 0.2 mM $CaCl_2$. Fluorescence lifetime and anisotropy decays were fit to a sum of exponentials using the method of nonlinear least squares, assuming frequency-independent errors in the phase delay and modulation of 0.2° and 0.005 as previously described in detail (*7*). Alternatively, in the case of fluorescence resonance energy transfer (FRET) measurements, data was also fit to a model that assumes a uniform Gaussian distribution of distances characterized by an average donor−acceptor separation (R_{av}) and half-width (HW) (*7, 44−46*), where the probability $P(r)$ of a particular spatial separation between donor and acceptor r is

$$P(r) = \exp\left[-\frac{1}{2}\left(\frac{r - R_{av}}{\sigma}\right)^2\right] \qquad (10)$$

The standard deviation of the distribution (σ) is related to the half-width of the distribution, where σ equals HW divided by 2.354.

RESULTS

Expression and Purification of Calmodulin Mutants. A mutant CaM ($CaMX^{145}$) lacking the last four amino acids Met^{145}-Thr^{146}-Ala^{147}-Lys^{148} at the carboxyl terminal was constructed through the substitution of a stop codon at the position encoding Met^{145}. To investigate the structure of the central helix, additional mutants involved the substitution of $Tyr^{99} \rightarrow Trp^{99}$ (Y99W) and $Leu^{69} \rightarrow Cys^{69}$ (L69C) for full-length CaM ($CaMC^{69}W^{99}$) or truncated CaM ($CaMC^{69}W^{99}X^{145}$) (Figure 1). All CaM species were expressed in *E. coli* and purified using the calcium-dependent changes in the hydrophobic interactions between CaM and phenyl-Sepharose CL-4B followed by weak anion exchange HPLC (*35*). A single peak with a retention time (t_R) of 22 min was observed and collected for both wild-type CaM and $CaMC^{69}W^{99}$ (Figure 2). However, two peaks were resolved for the sample containing either $CaMX^{145}$ or $CaMC^{69}W^{99}X^{145}$, with retention times of 22 and 28 min. To identify these species, we have used ESI mass spectrometry. The average

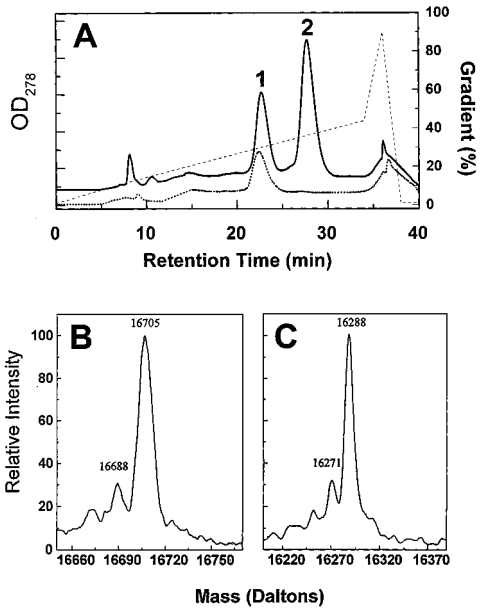

FIGURE 2: HPLC separation and ESI-MS identification of CaM. (A) Separation of wild-type vertebrate CaM (dotted line) and $CaMC^{69}W^{99}X^{145}$ (solid line) and (B, C) associated ESI-MS spectra after deconvolution of multiply charged ions of (B) wild-type CaM and (C) $CaMC^{69}W^{99}X^{145}$, corresponding to a CaM mutant involving the delection of the four carboxyl-terminal amino acids (i.e., Met^{145}-Thr^{146}-Ala^{147}-Lys^{148}) and substitution of $Tyr^{99} \rightarrow Trp^{99}$ and $Leu^{69} \rightarrow Cys^{69}$, as described in the text. Experimentally, CaM was separated using weak anion exchange HPLC, and 15 μg of CaM or $CaMC^{69}W^{99}X^{145}$ in 0.2 mM EGTA and 2% NH_4HCO_3 (pH 8.8) was trapped, desalted, and then directly infused (on-line) into an Autospec EQ mass spectrometer, essentially as previously described (*26*).

mass for wild-type CaM (t_r = 22 min) is 16 705 ± 3 Da (Figure 2B), consistent with the theoretical average mass expected for vertebrate CaM expressed in *E. coli* (i.e., 16 705.4 Da). A lower mass species (i.e., 16 690 ± 3 Da) corresponds to a charge-induced fragmentation artifact relating to the mass spectrometric conditions (*26*). The similar retention time (t_r = 22 min) of the first peak observed for the truncated clone suggests that a single stop codon engineered at position 145 was insufficient to fully terminate the transcription of the CaM gene. We have therefore collected the second peak (t_r = 28 min), which has an average mass of 16 288 ± 3 Da that is consistent with the expected average theoretical mass of 16 285.8 Da for $CaMC^{69}W^{99}X^{145}$ (Figure 2C). Additional resolution of the primary structure was obtained from a consideration of the tryptic peptides obtained from $CaMC^{69}W^{99}$ and from $CaMC^{69}W^{99}X^{145}$ (t_r = 28 min), which for the majority of peptides are identical for the two mutants. However, using reversed-phase HPLC, the retention time of the tryptic peptide associated with the carboxyl-terminal proteolytic fragment shifts from 79 min for native $CaMC^{69}W^{99}$ to 105 min upon deletion of Met^{145}-Lys^{148} in $CaMC^{69}W^{99}X^{145}$ (data not shown).

Calcium-Dependent Mobility Shifts Observed Using SDS−PAGE. The relative mobilities of apo- and calcium-saturated CaM using SDS−PAGE have previously been shown to provide a sensitive indication of conformational differences resulting from either site-directed amino acid substitutions or post-translational modifications (*27, 47, 48*). Wild-type CaM and $CaMC^{69}W^{99}$ exhibit similar mobilities using SDS−PAGE in both their apo- and calcium-saturated forms,

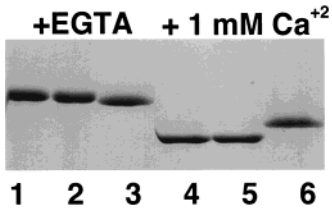

FIGURE 3: SDS−PAGE electrophoretic separation of CaM. Samples correspond to 5 μg of wild-type (lanes 1 and 3), CaMC^{69}W^{99} (lanes 2 and 5), or CaMC^{69}W^{99}X^{145} (lanes 3 and 6) in the presence of 10 mM EGTA (lanes 1−3) or 1 mM $CaCl_2$ using 15% (m/v) SDS−PAGE (*76*).

suggesting that substitution of Leu^{69} → Cys^{69} and Tyr^{99} → Trp^{99} does not perturb the calcium-dependent structural changes normally associated with calcium activation (Figure 3). This latter result is consistent with earlier data, demonstrating that wild-type CaM and CaMC^{69}W^{99} have similar calcium affinities and fully activate the PM−Ca−ATPase with similar CaM-binding affinities (*7*). However, while the relative mobility of CaMC^{69}W^{99}X^{145} in the apo form is similar to that of wild-type CaM and CaMC^{69}W^{99}, there is a substantial decrease in the mobility of calcium-saturated CaMC^{69}W^{99}X^{145} relative to full length CaM. These results suggest that deletion of Met^{145}-Lys^{148} results in substantial conformational differences following calcium activation.

Calcium-Binding Stoichiometry. To address whether conformational differences observed for CaMC^{69}W^{99}X^{145} following calcium activation may arise from the loss of a high-affinity calcium-binding site resulting from the deletion of Met^{145}-Lys^{148}, we have measured the stoichiometry of calcium binding using $^{45}CaCl_2$ and equilibrium dialysis. Using wild-type CaM, we find that 3.4 ± 0.4 mol of calcium bind/CaM, consistent with the presence of four high-affinity calcium-binding sites (*2*). In contrast, 2.4 ± 0.1 mol of calcium bind per mole of CaMC^{69}W^{99}X^{145}, indicating the loss of one high-affinity calcium-binding site upon deletion of Met^{145}-Lys^{148}.

Calcium-Dependent Activation of the PM−Ca−ATPase. Possible alterations in the functional properties of CaMC^{69}W^{99}X^{145} were assessed from a consideration of the ability to activate the PM−Ca−ATPase. Previous measurements have demonstrated that the calcium-dependent activation of the PM−Ca−ATPase by wild-type CaM and CaMC^{69}W^{99} are virtually identical, indicating that the substitution of Leu^{69} → Cys^{69} and Tyr^{99} → Trp^{99} has essentially no effect on CaM function. Prior to binding CaM, the calcium-dependent activation of the PM−Ca−ATPase can be described by assuming a single class of calcium-binding sites with a dissociation constant (k_d) of 2.4 ± 0.4 μM and a Hill coefficient (n_H) of 0.9 ± 0.2 (Figure 4A). This result is consistent with the fact that the PM−Ca−ATPase has a single high-affinity calcium-binding site (*49*). The addition of saturating concentrations of CaM results in an increase in the apparent calcium affinity and enhanced cooperativity (k_d = 0.68 ± 0.01 μM; n_H = 2.6 ± 0.1), with a corresponding 5-fold activation of the PM−Ca−ATPase. The observed increase in cooperativity is presumably a reflection of cooperative interactions associated with calcium binding to CaM in the presence of the PM−Ca−ATPase. A similar level of enzyme activation is observed for CaMC^{69}W^{99}X^{145}, indicating a retention of function following deletion of Met^{145}-Lys^{148}. However, in comparison to full-length CaM one observes a 4-fold increase in the calcium concentration necessary for half-maximal activation of the PM−Ca−ATPase in the presence of saturating concentrations of CaMC^{69}W^{99}X^{145} (i.e., k_d = 3.0 ± 0.1 μM). There is a corresponding decrease in the Hill coefficient (n_H = 1.9 ± 0.1), consistent with the loss of one high-affinity calcium-binding site.

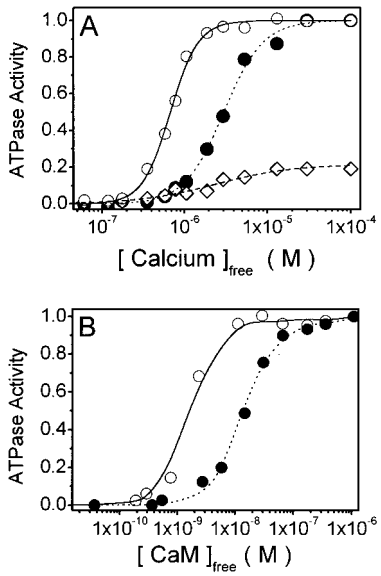

FIGURE 4: Functional activation of the PM−Ca-ATPase. Rates of ATP hydrolysis of the PM−Ca−ATPase were measured in the absence (◇) or presence of either wild-type CaM (○) or CaMC^{69}W^{99}X^{145} (●) in the presence of either 0.36 μM CaM (A) or 30 μM free calcium (B) at 37 °C, as described in Experimental Procedures. Experimental curves in *panel A* were obtained from a least-squares fit to eq 9 assuming A = 1.0. The least-squares fit for CaM was $k_d = 6.8 \pm 0.1 \times 10^{-7}$ M and $n = 2.6 \pm 0.1$ (○), for CaMC^{69}W^{99}X^{145} was $k_d = 3.0 \pm 0.1 \times 10^{-6}$ M and $n = 1.9 \pm 0.1$ (●), and for the PM−Ca−ATPase alone was $k_d = 2.4 \pm 0.4 \times 10^{-6}$ M and $n = 0.9 \pm 0.2$ (◇). Experimental curves in *panel B* were obtained from a least-squares fit to eq 7, where for CaM (○) $K_{d1} = 1.0 \pm 0.3 \times 10^{-8}$ M and $K_{d2} = 4 \pm 1 \times 10^{-10}$ M and for CaMC^{69}W^{99}X^{145} (●) $K_{d1} = 9 \pm 2 \times 10^{-8}$ M and $K_{d2} = 3 \pm 1 \times 10^{-10}$ M.

CaM-Dependent Activation of the PM−Ca−ATPase. To further investigate the functional effects of deleting Met^{145}-Lys^{148}, we have measured the CaM-dependent activation of the PM−Ca−ATPase by CaMC^{69}W^{99}X^{145} (Figure 4B). In comparison to native CaM, where $K[CaM]_{1/2} = 1.7 \pm 0.6$ nM, half-maximal activation of the PM−Ca−ATPase requires 8-fold more CaMC^{69}W^{99}X^{145} ($K[CaM]_{1/2} = 14.4 \pm 0.8$ nM). CaM has previously been shown to bind to the PM−Ca−ATPase in a sequential and cooperative manner, where the high-affinity binding of the carboxyl-terminal domain induces structural changes within the CaM-binding sequence to facilitate binding of the amino-terminal domain (*42*). Thus, the shift in the CaM-dependent activation of the PM−Ca−ATPase toward higher concentrations of CaMC^{69}W^{99}X^{145} could be the result of either (i) a decreased affinity between the carboxyl-terminal domain of CaMC^{69}W^{99}X^{145} and the PM−Ca−ATPase or (ii) alterations in cooperative interactions between binding sites on the opposing domains of CaMC^{69}W^{99}X^{145} that result in a diminished binding affinity between the amino-terminal domain and the CaM-binding sequence of the PM−Ca−ATPase relative to that observed using native CaM. To distinguish between these possibilities, we have fit theCaM-dependent activation of the PM−Ca−

ATPase by CaMC^{69}W^{99}X^{145} to eq 7 in Experimental Procedures, which explicitly considers binding interactions between both of the opposing globular domains of CaM in the activation of the PM−Ca−ATPase (*42*). In comparison to full-length CaM ($K_{d1} = 1.0 \pm 0.3 \times 10^{-8}$ M; $K_{d2} = 4 \pm 1 \times 10^{-10}$ M), there is a 9-fold increase in the dissociation constant between the carboxyl-terminal domain of CaMC^{69}W^{99}X^{145} ($K_{d1} = 9 \pm 2 \times 10^{-8}$ M) with little or no change in the subsequent binding affinity of the amino-terminal domain ($K_{d2} = 3 \pm 1 \times 10^{-10}$ M). These latter results suggest that structural changes within the carboxyl-terminal domain are responsible for the shift toward higher concentrations in the CaM-dependent activation of CaMC^{69}W^{99}X^{145}. However, the ability of micromolar concentrations of CaMC^{69}W^{99}X^{145} to fully activate the PM−Ca−ATPase indicates that structural alterations induced by deletion of Met^{145}-Lys^{148} does not result in any alteration in the ability of CaMX^{145} to bind and activate the PM−Ca−ATPase, suggesting that target protein binding rescues the native-like conformation of CaM. This latter result is consistent with earlier results in which normal binding interactions between conformationally altered CaM mutants have been shown to be restored upon binding to target proteins (*32*−*34*).

Circular Dichroism Measurements of Secondary Structure. The four amino acids between Met^{145} and Lys^{148} are expected to stabilize the carboxyl-terminal α-helix between Tyr^{138} and Thr^{146}, which represents about 6% of the α-helical content in CaM (*2*). In addition, proximal interactions involving this helix may function to stabilize both the four-helix bundle within the carboxyl-terminal domain and the central helix (Figure 1) (*2, 5*). Therefore, CD spectroscopy was used to determine the effect of deleting the four amino acids at the carboxyl-terminal of CaM on the α-helical content. There is a small decrease in the ellipticity of CaM following calcium binding, consistent with earlier suggestions that calcium binding results in a reorientation of secondary structural elements with respect to one another (*50*−*53*). Fitting the data indicates that calcium-activated CaMC^{69}W^{99} contains approximately 66 ± 3% α-helix, which is consistent with the crystal structure (*2, 29*). One observes a large increase in the molar ellipticity for CaMC^{69}W^{99}X^{145} in comparison to that for CaMC^{69}W^{99} for both apo- and calcium-saturated CaM (Figure 5), suggesting that deletion of Met^{145}-Lys^{148} results in a substantial decrease in the α-helical content. Fitting the data for CaMC^{69}W^{99}X^{145} following calcium activation indicates that there is approximately 35 ± 1% α-helical content. Thus, deletion of the carboxyl-terminal four amino acids results in a large decrease in the secondary structure of CaMC^{69}W^{99}X^{145}, indicating that there are global structural changes resulting from the absence of normal stabilizing interactions involving the carboxyl-terminal sequence. Calcium binding results in a similar increase in the apparent α-helical content of CaMC^{69}W^{99}X^{145} to that observed for full-length CaM (i.e., CaMC^{69}W^{99}). These results indicate that CaM adopts a new structure following deletion of Met^{145}-Lys^{148} that preserves calcium-dependent structural changes involving secondary structural elements that are normally associated with calcium binding in native CaM. Thus, deletion of the last four amino acids in the carboxyl-terminal domain results in large structural changes that arise as a result of the loss of stabilizing interactions between these side chains and other structural elements in CaM.

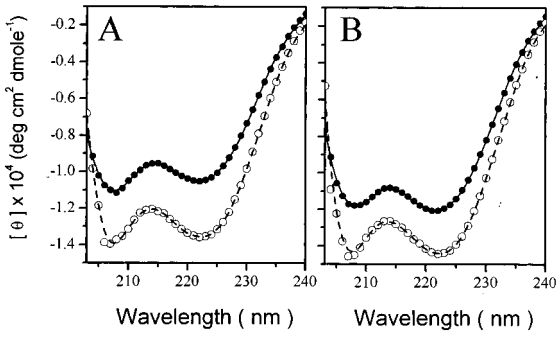

FIGURE 5: Circular dichroism spectra. Experimental data corresponding to CaMC^{69}W^{99} (○) or CaMC^{69}W^{99}X^{145} (●) in the presence of either 1 mM EGTA (A) or 0.1 mM Ca(ClO$_4$)$_2$ (B). Lines correspond to least-squares fits obtained using the program Contin (*43*) to estimate α-helical content for CaMCW and CaMX^{145}, which were respectively determined to be 63 ± 3% and 31 ± 1% for apo-CaM and 66 ± 3% and 35 ± 1% for calcium-saturated CaM. Experimental conditions involved 2 μM CaM in 10 mM Tris−HCl (pH 7.5), 0.1 M KClO$_4$, 1 mM Mg(ClO$_4$)$_2$, and the indicated amounts of either EGTA or Ca(ClO$_4$)$_2$ at 25 °C.

Estimation of Calcium-Binding Affinities. The fluorescence intensity associated with Trp^{99} has previously been demonstrated to be sensitive to calcium binding to sites in the amino- and carboxyl-terminal domains (*7*) and provides a convenient means to assess possible changes in the structural coupling between the opposing globular domains of CaM resulting from deletion of Met^{145}-Lys^{148}. Since Trp^{99} is substituted for Tyr^{99} in wild-type CaM, whose carbonyl group contributes to calcium-binding site 3 in the crystal structure of CaM (*2*), it is likely that Trp^{99} preferentially senses high-affinity calcium binding at this site. The quantum yield of Trp^{99} in CaMC^{69}W^{99}X^{145} is substantially less than that of CaMC^{69}W^{99} prior to calcium binding (Figure 6), suggesting that there are substantial conformational differences. However, following calcium binding, the fluorescence quantum yield of Trp^{99} is very similar for both CaMC^{69}W^{99} and CaMC^{69}W^{99}X^{145}. These results indicate that calcium binding restores the native conformation in the vicinity of calcium-binding site 3 and that the large decrease in α-helical content, apparent from the CD spectra in Figure 5, arises as a result of the destabilization of a spatially distant portion of CaM.

Additional information concerning possible differences in the structural coupling between calcium-binding sites in the amino- and carboxyl-terminal domains of CaM is possible from a consideration of the calcium dependence of changes in the quantum yield of Trp^{99}. The fluorescence response of Trp^{99} in CaMC^{69}W^{99} is biphasic, consistent with previous results that have demonstrated a structural coupling between calcium binding to sites in the amino- and carboxyl-terminal domains of CaM (*6, 9, 31*). In vertebrate CaM the calcium-binding sites in the carboxyl-terminal domain are known to have a higher calcium-binding affinity in comparison with the sites in the amino-terminal domain (*55*−*57*). Therefore, the sensitivity of the quantum yield of Trp^{99} to both classes of calcium-binding sites suggests that global structural changes are sensed in the vicinity of Trp^{99} upon calcium occupancy of sites in either the amino- or carboxyl-terminal domains. The calcium-dependent change in the quantum yield of CaMC^{69}W^{99} can be adequately described by eq 9, involving two terms that are individually similar to those in the Hill equation. The first class of calcium-binding sites

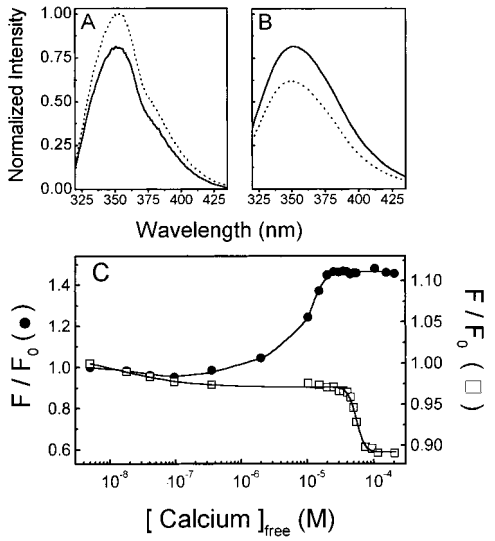

FIGURE 6: Calcium-dependent changes in the fluorescence intensity of Trp^{99}. Fluorescence emission spectra are shown for the apo- (dotted line) and calcium-saturated (solid line) forms of $CaMC^{69}W^{99}$ (A) and $CaMC^{69}W^{99}X^{145}$ (B). Calcium-dependent spectral changes in the maximal fluorescence intensity (F) relative to that observed in the presence of 5 nM free calcium (F_0) of $CaMC^{69}W^{99}X^{145}$ (●) and $CaMC^{69}W^{99}$ (□) are shown in panel C, where lines represent the least-squares fit to eq 9 in Experimental Procedures. Fitting parameters for $CaMC^{69}W^{99}X^{145}$ are $A = 0.12 \pm 0.03$, $k_{d1} = 6 \pm 4 \times 10^{-8}$ M, $n_1 = 0.9 \pm 0.6$, $k_{d2} = 1.1 \pm 0.1 \times 10^{-5}$ M, and $n_2 = 4.2 \pm 0.4$. Fitting parameters for $CaMC^{69}W^{99}$ are $A = 0.06 \pm 0.03$, $k_{d1} = 2 \pm 2 \times 10^{-8}$ M, $n_1 = 0.8 \pm 0.4$, $k_{d2} = 5.4 \pm 0.1 \times 10^{-5}$ M, and $n_2 = 8 \pm 1$. Experimental conditions involved 6 μM protein in 0.1 M HEPES (pH 7.5), 0.1 M KCl, 0.1 mM EGTA, and sufficient $CaCl_2$ to yield the indicated free calcium concentration, which was directly measured as previously described (*58*).

($k_{d1} = 20 \pm 20$ nM; $n_1 = 0.8 \pm 0.4$) is associated with a 3% decrease in fluorescence. Calcium occupancy of a secondary class of binding sites results in an additional 8% decrease in fluorescence intensity ($k_{d2} = 54 \pm 10$ μM; $n_2 = 8 \pm 1$) (Figure 6C). These results are consistent with previous measurements in which occupancy of the lower affinity class of calcium-binding sites in the amino-terminal domain, with an apparent affinity of approximately 40 μM, have been shown to induce global structural changes (*6, 8, 9, 21, 54, 58*). Thus, the computed dissociation constants (i.e., k_{d1} and k_{d2}) obtained from a consideration of calcium-dependent changes in the fluorescence of Trp^{99} are expected to provide an accurate assessment of their relative calcium affinities, since they reflect global structural changes resulting form calcium occupancy of the low- and high-affinity calcium-binding sites. In contrast, the actual values of the exponents (n) provide only a qualitative index of the structural coupling between calcium-binding sites and are not expected to reliably indicate the number of sites associated with either class of calcium-binding sites, since changes in the quantum yield of Trp^{99} result from structural changes in the proximity of Trp^{99}. In this latter respect, the substantially larger exponential coefficient (n_2) associated with calcium occupancy to the lower affinity class of calcium sites relative to the high-affinity class of sites (n_1) in $CaMC^{69}W^{99}$ is not an indication of differences in the number of calcium-binding sites. Rather, these results suggest that occupancy of all four calcium-binding sites is needed to induce highly cooperative structural changes involving many intramolecular interactions in the vicinity of Trp^{99}. Therefore, at higher calcium concentrations, Trp^{99} is responding to concerted structural changes involving both CaM domains.

In comparison to $CaMC^{69}W^{99}$, we find that $CaMC^{69}W^{99}X^{145}$ also exhibits biphasic fluorescence changes associated with two classes of calcium-binding sites. The higher affinity class of site(s) has a comparable affinity to that observed for $CaMC^{69}W^{99}$ and results in a similar reduction in fluorescence intensity to that of full-length CaM (i.e., $k_{d1} = 60 \pm 40$ nM; $n_1 = 0.9 \pm 0.6$), suggesting that there are no intrinsic differences with respect to the mechanisms of calcium activation in the vicinity of calcium-binding site 3. The value associated with the exponent in the fitting equation to the high-affinity class of calcium-binding sites is much less than the positive Hill coefficients obtained from direct measurements of calcium binding for full length CaM, which have previously indicated the presence of positive cooperativity between the high-affinity class of calcium-binding sites (*59*). Since alterations in the fluorescence quantum yield of Trp^{99} directly report structural changes in the vicinity of calcium-binding site 3, these results suggest that occupancy of calcium-binding site 3 may function to induce binding to site 4 in native calmodulin. Consistent with this latter interpretation, observed changes in the fluorescence intensity of Trp^{99} associated with occupancy of the high-affinity class of calcium-binding sites are similar in $CaMC^{69}W^{99}$ and $CaMC^{69}W^{99}X^{145}$, although one calcium-binding site (presumably site 4) is lost in $CaMX^{145}$. However, in contrast to the similar fluorescence responses associated with high-affinity calcium binding to $CaMC^{69}W^{99}$ and $CaMC^{69}W^{99}X^{145}$, in comparison to full-length CaM occupancy of the lower-affinity class of calcium-binding sites (i) results in a large enhancement in fluorescence intensity, (ii) occurs at a lower calcium concentration, and (iii) exhibits a reduced cooperativity (i.e., $k_{d2} = 11 \pm 1$ μM; $n_2 = 4.2 \pm 0.4$). The enhanced calcium-binding affinity relative to full length CaM suggests that structural interactions involving the carboxyl-terminal sequence normally function to reduce the calcium-binding affinity. This result is consistent with earlier measurements obtained using yeast CaM where deletion of amino acids 133−148 also results in an enhanced calcium-binding affinity (*19*). With respect to differences in the calcium concentration necessary for half-maximal activation of the PM−Ca−ATPase by CaM (Figure 4) relative to that needed for the titration of calcium-binding sites in CaM (Figure 6C), it is apparent that the presence of the PM−Ca−ATPase reduces the concentration of calcium necessary for activation of CaM and the associated increase in the transport activity of the PM−Ca−ATPase to a larger extent for CaMCW relative to that observed for $CaMX^{145}$ (Figure 4B). These results indicate that additional steps not apparent from a consideration of the calcium-dependent activation of isolated calmodulin are important with respect to activation of the PM−Ca−ATPase, which includes calmodulin binding and the structural changes that result in the activation of the PMCA. Indeed, changes in the structural coupling between the opposing globular domains in $CaMX^{145}$ revealed in Figure 6C must be overcome to induce the enzyme activation demonstrated in Figure 4.

Fluorescence Lifetime Measurements. Changes in the pre-exponential amplitudes of the three major fluorescence lifetimes associated with individual tryptophans in proteins can reveal additional details regarding localized secondary

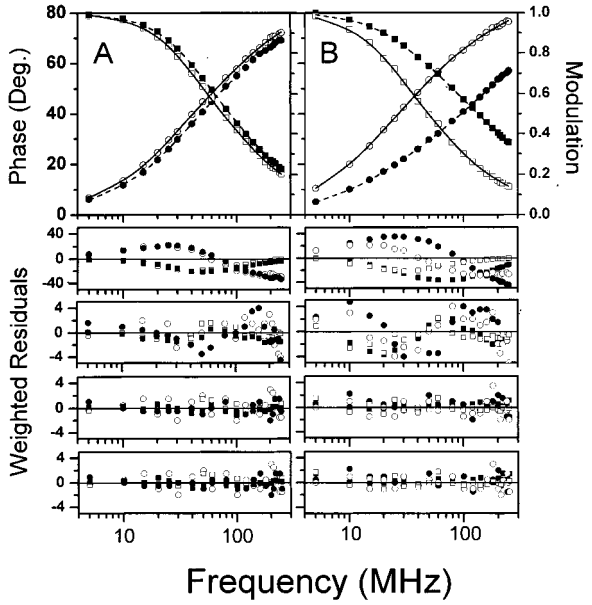

FIGURE 7: Lifetime-resolved fluorescence intensity decays for Trp^{99}. The frequency response of the phase shift (○, ●) and modulation (□, ■) for Trp^{99} is shown for $CaMC^{69}W^{99}X^{145}$ in the absence (○, □) and in the presence (●, ■) of AEDANS bound to Cys^{69}. Experimental conditions involved 6 μM $CaMC^{69}W^{99}X^{145}$ in buffer B in the absence (A) or in the presence (B) of 0.2 mM $CaCl_2$. Lines represent the experimental fit to a three-exponential decay. Weighted residuals are shown below the frequency-domain data for various models which, from top to bottom, correspond to one-, two-, three-, and four-exponential fits to the data. Weighted residuals correspond to the difference between the experimental data and the calculated fit divided by the standard error of the individual measurements, which was assumed to be 0.2° and 0.005 for the phase and modulation data, respectively.

structural changes, as the relative contribution of different rotomers of tryptophan has been demonstrated to be differently constrained by side-chain interactions within different protein secondary structures (*60, 61*). We have therefore measured the fluorescence lifetime intensity decay of Trp^{99} in apo- and calcium-activated $CaMC^{69}W^{99}$ and $CaMC^{69}W^{99}X^{145}$ using frequency domain fluorescence spectroscopy (Figure 7). As previously described for a range of different proteins, the intensity decays of Trp^{99} in either $CaMC^{69}W^{99}$ or $CaMC^{69}W^{99}X^{145}$ can be adequately described as a sum of three exponentials, as indicated by the weighted residuals that are randomly distributed about the origin. In comparison to $CaMC^{69}W^{99}$, the individual lifetime components in $CaMC^{69}W^{99}$ X^{145} become somewhat shorter (Table 2), suggesting differences in the local environment. However, there are substantial differences in the pre-exponential amplitudes (i.e., α_i; Table 2), which is a reflection of large differences in conformational constraints associated with the side-chain dynamics of tryptophan (*60*). Since Trp^{99} replaces Tyr^{99}, which is greater than 12 Å from any side chains in the carboxyl-terminal α-helix located between Tyr^{138} and Thr^{146} in the crystal structure (*2, 29*), these results provide additional support that deletion of Met^{145}-Lys^{148} results in global structural changes involving the entire carboxyl-terminal domain.

Solvent Accessibility. Additional resolution of changes in the conformation around Trp^{99} is possible through a consideration of the solvent accessibilities of Trp^{99} to the collisional quencher acrylamide. In agreement with high-resolution structural data that suggests conformational

Table 2: Lifetime Data for Trp^{99} in the Absence (D) and Presence (D−A) of AEDANS Covalently Bound to Cys^{69} [a]

sample	α_1	τ_1 (ns)	α_2	τ_2 (ns)	α_3	τ_3 (ns)	$\bar{\tau}$ [b] (ns)	χ_R^2
				+ EGTA				
$CaMC^{69}W^{99}$ [c]								
D	0.27	1.1	0.23	3.2	0.50	5.9	4.0	1.5
	(0.04)	(0.1)	(0.07)	(0.07)	(0.03)	(0.1)	(0.1)	
D−A	0.29	1.1	0.30	3.8	0.41	5.8	3.8	1.5
	(0.01)	(0.1)	(0.02)	(0.2)	(0.01)	(0.1)	(0.1)	
$CaMC^{69}W^{99}$ X^{145}								
D	0.24	0.2	0.40	1.7	0.36	4.8	2.5	1.1
	(0.08)	(0.1)	(0.04)	(0.1)	(0.04)	(0.1)	(0.2)	
D−A	0.29	0.6	0.44	2.1	0.27	4.6	2.3	0.9
	(0.02)	(0.1)	(0.01)	(0.2)	(0.03)	(0.2)	(0.1)	
				+ Calcium				
$CaMC^{69}W^{99}$ [c]								
D	0.39	1.3	0.45	2.6	0.16	8.0	2.9	1.6
	(0.08)	(0.1)	(0.05)	(0.3)	(0.03)	(0.5)	(0.1)	
D−A	0.44	1.2	0.41	2.5	0.15	7.3	2.6	2.2
	(0.03)	(0.1)	(0.02)	(0.1)	(0.01)	(0.3)	(0.1)	
$CaMC^{69}W^{99}X^{145}$								
D	0.36	0.1	0.33	2.4	0.31	7.2	3.1	1.3
	(0.01)	(0.1)	(0.01)	(0.2)	(0.01)	(0.1)	(0.1)	
D−A	0.55	0.5	0.37	1.6	0.08	5.7	1.3	0.9
	(0.01)	(0.1)	(0.01)	(0.1)	(0.01)	(0.2)	(0.1)	

[a] Average amplitudes (α_i) and lifetimes (τ_i) obtained from three-exponential fits to frequency domain data for the time-dependent intensity decay, $I(t)$, for Trp^{99} in the absence (D) and presence (D−A) of AEDANS bound to Cys^{69}, assuming $I(t) = \sum_i \alpha_i e^{-t/\tau i}$. [b] $\bar{\tau} = \sum \alpha_i \tau_i$. [c] Data from ref *7*. Errors represent standard error of the mean for three to four measurements. Experimental conditions include 6 μM CaM in buffer **B** in the absence (+EGTA) or in the presence (+Calcium) of 0.2 mM $CaCl_2$. Temperature was 25 °C.

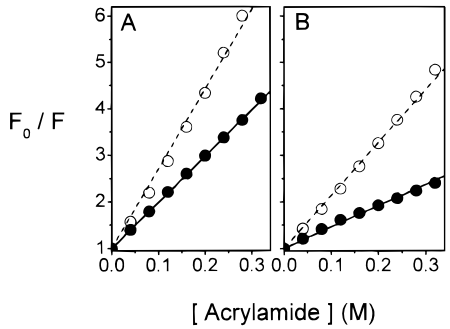

FIGURE 8: Solvent accessibilities of Trp^{99}. Stern−Volmer plots of Trp^{99} for apo- (A) or calcium-activated (B) $CaMC^{69}W^{99}$ (○) or $CaMC^{69}W^{99}X^{145}$ (●). Experimental conditions are as described in Figure 7. Emission was detected at 350 nm. Additional details are provided in the legend to Table 3.

rearrangements of helical elements result in a reduced solvent accessibility of Tyr^{99} following calcium activation (*29, 62*), we find that the solvent accessibility of Trp^{99} located at the analogous position in $CaMC^{69}W^{99}$ becomes smaller following calcium activation (Figure 8, Table 3). A similar reduction in the solvent accessibility of Trp^{99} is observed in $CaMC^{69}W^{99}X^{145}$ upon calcium activation, indicating that calcium-dependent structural changes are preserved in the carboxyl-terminal domain. However, relative to $CaMC^{69}W^{99}$ there is a substantial decrease in the solvent accessibilities of Trp^{99} for both apo- and calcium-activated $CaMC^{69}W^{99}X^{145}$, suggesting that deletion of Met^{145}-Lys^{148} results in global structural changes within the entire carboxyl-terminal domain that induce the formation of a more closed structure.

Table 3: Stern-Volmer Quenching Constants[a]

sample	$\langle\tau\rangle$ (ns)[b]	K_{sv} (M^{-1})[c]	k_q (M^{-1} s^{-1}) $\times 10^{-9}$ [d]	k_q/k_q (free)[e]
		+EGTA		
$CaMC^{69}W^{99}$	5.0 ± 0.1	17.6 ± 0.3	3.52 ± 0.09	0.60 ± 0.02
$CaMC^{69}W^{99}X^{145}$	3.9 ± 0.5	10.0 ± 0.1	2.6 ± 0.3	0.44 ± 0.05
		+Calcium		
$CaMC^{69}W^{99}$	4.8 ± 0.1	11.6 ± 0.1	2.42 ± 0.05	0.41 ± 0.01
$CaMC^{69}W^{99}X^{145}$	5.9 ± 0.3	4.5 ± 0.1	0.76 ± 0.04	0.13 ± 0.01

[a] Protein conformational changes are revealed by changes in solvent accessibility of the water-soluble quencher, acrylamide, to Trp^{99} in CaM. [b] $\langle\tau\rangle = \sum\alpha_i\tau_i^2/\sum\alpha_i\tau_i$ (see Table 2). [c] Stern−Volmer quenching constant (K_{sv}) is obtained from monitoring the Trp^{99} fluorescence emission change at 352 nm, where $F_0/F = 1 + K_{sv}$ [acrylamide]. [d] Bimolecular quenching constant (k_q) equals $K_{sv}/\langle\tau\rangle$. [e] Solvent accessibility normalized to *N*-acetyl-L-tryptophanamide (NATA) in solution, where k_q(NATA) $= 5.9 \times 10^9$ M^{-1} s^{-1} (*74*). Sample conditions are as described in the legend to Figure 7.

Alternatively, enhanced interactions between opposing domains could account for the reduced solvent accessibility.

Spatial Separation between Opposing Globular Domains. Yeast CaM adopts a more compact structure in comparison to vertebrate CaM, and conformational interactions between the opposing domains are associated with calcium binding to either yeast CaM or mutants of *Drosophila* that lack calcium-binding site 4 (*18, 19, 21, 63,* 64). Since $CaMC^{69}W^{99}X^{145}$ also lacks one high-affinity calcium-binding site, it is of interest to determine whether deletion of Met^{145}-Lys^{148} results in large changes in the proximity between the opposing globular domains. To measure the spatial separation between the two opposing domains in CaM, we used a pair of chromophores at sites near the opposite ends of the central helix, located between Glu^{67} and Phe^{92}, that have overlapping absorption and fluorescence emission spectra. Trp^{99} serves as a fluorescence resonance energy transfer (FRET) donor, while AEDANS bound to Cys^{69} acts as a FRET acceptor (Figure 1). The modified CaM can activate the PM−Ca−ATPase fully, suggesting that AEDANS labeling results in minimal structural or functional perturbations (*7*). In the calculation of the apparent spatial separation (r_{app}) between the opposing ends of the central helix, we have assumed that the orientation between donor and acceptor chromophores is motionally averaged (i.e., $\kappa^2 = 2/3$). As previously discussed, the multiple absorption transition dipoles and small steady-state polarization values associated with AEDANS coupled with the rapid rotational dynamics of these chromophores on the nanosecond time scale suggest that errors in the calculation of distances between Trp^{99} and AEDANS bound to Cys^{69} on either $CaMC^{69}W^{99}$ or $CaMC^{69}W^{99}X^{145}$ are no larger than 3 Å (see below) (*7, 44, 46, 65*).

In all cases the presence of AEDANS decreases the fluorescence intensity of Trp^{99} ($\lambda_{em} \approx 350$ nm). There are corresponding increases in the fluorescence emission of AEDANS ($\lambda_{em} \approx 490$ nm), indicating the presence of FRET (Figure 9). Likewise, in the presence of AEDANS, the frequency response of Trp^{99} is shifted toward higher frequencies, indicating that the average fluorescence lifetime is reduced (Figure 7). The FRET efficiencies calculated from the reduction in the mean lifetime are virtually identical to that calculated from steady-state measurements (Tables 2 and 4). Thus, no static component is present in the measured

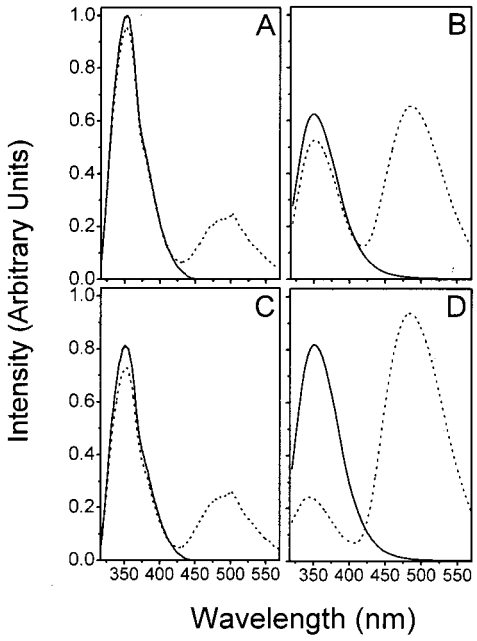

FIGURE 9: Steady-state measurements of fluorescence resonance energy transfer. Fluorescence intensities of Trp^{99} for apo- (A, B) and calcium-saturated (C, D) $CaMC^{69}W^{99}$ (A, C) or $CaMC^{69}W^{99}X^{145}$ (B, D) in the absence (solid line) and in the presence (dotted line) of the FRET acceptor AEDANS. Experimental conditions are as described in the legend to Figure 7. Spectra were arbitrarily normalized to unity for apo-$CaMC^{69}W^{99}$ in the absence of bound AEDANS. Excitation was at 297 nm using a Xenon lamp, and all slit widths were set at 4 nm. Temperature was 25 °C.

FRET efficiency that would result from a significant population of chromophores with a donor−acceptor separation less than $0.5 \times R_0$ (i.e., less than 11 Å). There is a substantial increase in FRET for calcium-activated CaM, which increases from $13 \pm 3\%$ for native CaM to $64 \pm 4\%$ upon deletion of the carboxyl-terminal four amino acids. These results indicate that deletion of Met^{145}-Lys^{148} results in a smaller average donor−acceptor separation between chromophores located on the opposing globular domains near the ends of the central helix, which for calcium-activated CaM decreases from an apparent spatial separation (r_{app}) of 30 ± 1 Å for $CaMC^{69}W^{99}$ to 20 ± 1 Å for $CaMC^{69}W^{99}$ (Table 4). A similar decrease in the apparent spatial separation between these chromophores is observed for apo-CaM. However, from these results it is unclear whether the smaller average spatial separation between the opposing domains in $CaMC^{69}W^{99}X^{145}$ is the result of the disruption of the central helix, which would result in the dynamic structural uncoupling of the opposing domains, or the adoption of a unique structure bringing the opposing domains into closer proximity. To address this latter question, we have used the frequency domain intensity decays of Trp^{99} in the absence and presence of AEDANS bound to Cys^{69} to resolve the conformational heterogeneity between chromophores located on the opposing globular domains (Figure 7). These data are typically analyzed in terms of a uniform Gaussian distribution of distances with an average spatial separation (R_{av}) and half-width (HW) (Table 4). This model has previously been successfully used to describe the conformational heterogeneity of a range of different macromolecules, including CaM (*7, 44*−*46, 58*). Furthermore, the observed conformational heterogeneity within the central

Table 4: Spatial Separation between Trp^{99} and AEDANS Bound to Cys^{69} [a]

sample	$\bar{\tau}_d$ (ns)	$\bar{\tau}_{da}$ (ns)	E%[c]	R_0[b] (Å)	r_{app}[b] (Å)	R_{av}[c] (Å)	HW[c] (Å)	χ_R^2
				+EGTA				
$CaMC^{69}W^{99}$ [d]	4.0	3.8	7	23.8	37	38	<16	2.1
	(0.1)	(0.1)	(1)	(0.1)	(2)	(37−43)		
$CaMC^{69}W^{99}X^{145}$	2.5	2.3	9	21.1	31	29	10	1.4
	(0.2)	(0.1)	(6)	(0.1)	(4)	(28.3−30.2)	(2−13)	
				+Calcium				
$CaMC^{69}W^{99}$ [d]	2.9	2.6	15	22.6	30	31	<10	1.8
	(0.1)	(0.1)	(3)	(0.1)	(1)	(30−32)		
$CaMC^{69}W^{99}X^{145}$	3.1	1.3	64	22.1	20	17.7	3.6	2.2
	(0.1)	(0.1)	(4)	(0.1)	(1)	(17.4−18.0)	(3.1−4.0)	

[a] Distance obtained from fluorescence resonance energy transfer (FRET) measurements between Trp^{99} and AEDANS attached at Cys^{69} in CaM. [b] Observed energy-transfer efficiency (E) is obtained as

$$E = 1 - \frac{\bar{\tau}_{da} - \bar{\tau}_d \times (1 - f_a)}{\bar{\tau}_d \times f_a} = \frac{R_0^6}{R_0^6 + r_{app}^6}$$

E is the corrected fluorescence resonance energy-transfer efficiency that takes into account the incomplete labeling of AEDANS at Cys^{69} (i.e., $f_a = 0.91 \pm 0.02$), $\bar{\tau}_d$ is the mean lifetime of Trp^{99}, $\bar{\tau}_{da}$ is the mean lifetime of Trp^{99} in the presence of AEDANS at Cys^{69}, R_0 is the Förster critical distance that is obtained under a given set of experimental conditions, r_{app} is the apparent spatial separation between Trp^{99} and AEDANS at Cys^{69}. [c] Average donor−acceptor separation (R_{av}) and associated half-width (HW) assuming a uniform Gaussian distribution of distances between donor and acceptor chromophores (see eq 10 in Experimental Procedures), where indicated errors (in brackets) were obtained from a global analysis of errors, as depicted in Figure 10. Errors in other parameters are standard errors of the mean for three independent measurements. [d] Data for $CaMC^{69}W^{99}$ are taken from ref *7*.

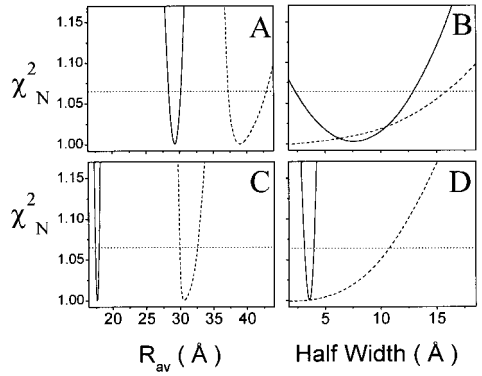

FIGURE 10: Depiction of error surfaces for Gaussian distance distribution model. Parameter values were obtained from a simultaneous fit to more than three independent data sets to recover the average spatial separation (R_{av}; A and C) and half-width (B and D) for a model involving a Gaussian distribution of distances between donor (Trp^{99}) and acceptor (i.e., AEDANS covalently bound to Cys^{69}) for $CaMC^{69}W^{99}$ (dotted line) and $CaMC^{69}W^{99}X^{145}$ (solid line) for apo- (A, B) and calcium-saturated (C, D) CaM. Experimental values (i.e., R_{av} or half-width) were incrementally adjusted, and all other parameters were allowed to vary in the least-squares analysis, essentially as previously described (*7*). The horizontal line corresponds to the F statistic for one standard deviation. Experimental conditions are as described in the legend to Figure 7.

helix of full-length CaM is consistent with earlier NMR results, which also indicate the presence of considerable conformational heterogeneity (*13*, *66*).

Upon fitting the fluorescence intensity decay data in Figure 7 to a model that assumes a uniform Gaussian distance distribution between donor and acceptor chromophores, we find that the structures of both apo- and calcium-activated $CaMC^{69}W^{99}X^{145}$ are conformationally distinct. In both cases, the half-widths (HW) associated with the Gaussian distance distribution are comparable or smaller than that observed for $CaMC^{69}W^{99}$ (Figure 10, Table 4). Furthermore, the average donor−acceptor distance (R_{av}) for both apo- and calcium-activated CaM are analogous to the results obtained assuming a single population of donor−acceptor distances calculated from the decrease in the mean fluorescence lifetimes (i.e., r_{app}, Table 4). Thus, irrespective of the model used to analyze the data, deletion of the carboxyl-terminal four amino acids results in a substantial decrease in the average spatial separation between chromophores near the ends of the central helix, corresponding to 6−9 Å for apo-CaM and 10−13 Å following calcium activation. Thus, deletion of Met^{145}-Lys^{148} and the associated loss of one high-affinity calcium-binding site in $CaMC^{69}W^{99}X^{145}$ results in the stabilization of conformationally distinct structures that bring the opposing globular domains into closer proximity in comparison to full-length CaM.

Hydrodynamic Properties of CaM. Measurements of the rotational dynamics of CaM provide a sensitive measure of the structural coupling between the opposing globular domains. At 25 °C the rotational correlation times associated with the independent rotational motion of the amino- or carboxyl-terminal domains of CaM are approximately 6−7 ns, while the rotational correlation time associated with the overall rotational motion of the entire molecule is approximately 11−12 ns (*13*, *58*, *67*, *68*). Therefore, additional information regarding possible changes in the structural coupling between the opposing globular domains resulting from deletion of the four carboxyl-terminal amino acids in $CaMC^{69}W^{99}X^{145}$ is possible through the measurement of the rotational dynamics. We have therefore measured the differential phase and modulated anisotropy of AEDANS bound to Cys^{69} in $CaMC^{69}W^{99}X^{145}$ at 20 frequencies between 2 and 100 MHz (Figure 11). The frequency response of both apo- (data not shown) and calcium-activated forms of $CaMC^{69}W^{99}X^{145}$ can be adequately described by two rotational correlation times. The longer rotational correlation time (i.e., $\phi_2 \approx 12$ ns) is associated with the global rotational motion of both apo- and calcium-activated CaM (*7*) and is very similar for $CaMC^{69}W^{99}$ and $CaMC^{69}W^{99}X^{145}$ (Table 5). The amplitude term associated with the relative contribution of overall protein rotational motion to the total anisotropy decay (i.e., $g_2 r_0$) is increased upon deletion of the last four amino acids at the carboxyl terminal, suggesting an enhanced structural coupling between the opposing globular domains. In contrast, the rate of segmental rotational motion of

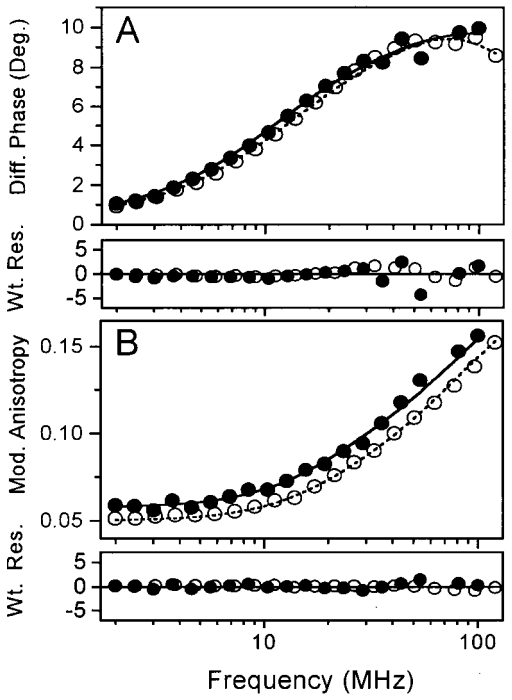

FIGURE 11: Rotational dynamics of CaM. Frequency responses (●, ○) and associated two-exponential fits (lines) of the differential phase (A) and modulated anisotropy (B) for AEDANS bound to Cys^{69} in $CaMC^{69}W^{99}X^{145}$ (●, solid line) or $CaMC^{69}W^{99}$ (○, dotted line). Weighted residuals (Wt. Res.) represent the difference between experimental and calculated data, normalized by the frequency-independent errors in the differential phase and modulated anisotropy, which were respectively assumed to be 0.2° and 0.005. Excitation was at 333 nm, and the emitted light was collected after a Schott GG400 long-pass filter. Experimental conditions are as described in the legend to Figure 7.

Table 5: Rotational Dynamics of AEDANS Bound to Cys^{69} in CaM[a]

sample	P	g_1r_0	ϕ_1 (ns)	g_2r_0	ϕ_2 (ns)	χ_R^2
			+EGTA			
$CaMC^{69}W^{99}$ [b]	0.078	0.109	1.9	0.087	13	0.5
	(0.001)	(0.002)	(0.3)	(0.002)	(1)	
$CaMC^{69}W^{99}X^{145}$	0.096	0.154	1.1	0.109	11	2.6
	(0.003)	(0.005)	(0.1)	(0.004)	(1)	
			+Calcium			
$CaMC^{69}W^{99}$ [b]	0.073	0.114	1.9	0.076	12	0.6
	(0.001)	(0.003)	(0.2)	(0.003)	(1)	
$CaMC^{69}W^{99}X^{145}$	0.088	0.114	1.3	0.104	12	4.3
	(0.002)	(0.002)	(0.1)	(0.001)	(1)	

[a] Indicated values and associated standard errors of the mean (in parentheses) for three independent measurements were obtained from a two-exponential fit to frequency-domain data collected for AEDANS bound to Cys^{69}, where the time dependence of the anisotropy decay, $r(t)$, equals $r_0(g_1e^{-t/\phi i} + g_2e^{-t/\phi 2})$. r_0 is the limiting anisotropy in the absence of rotational diffusion, ϕ_i are the rotational correlation times, and g_i is the associated pre-exponential amplitude. P is the steady-state polarization. [b] Data obtained from ref *7*. Experimental conditions are as described in the legend to Figure 7.

AEDANS bound to Cys^{69} (i.e., ϕ_1) is increased upon deletion of Met^{145}-Lys^{148}, as indicated by the shorter rotational correlation time (Table 5). These latter results suggest that deletion of the last four amino acids at the carboxyl terminal results in structural changes within the amino-terminal domain that reduce steric constraints associated with the segmental rotational motion of AEDANS.

Table 6: Rotational Dynamics of Trp^{99} in CaM[a]

sample	P	g_1r_0	ϕ_1 (ns)	g_2r_0	ϕ_2[b] (ns)	χ_R^2
			+EGTA			
$CaMC^{69}W^{99}$ [c]	0.21	0.08	1.2	0.20	⟨13⟩	0.8
	(0.01)	(0.02)	(0.2)	(0.01)		
$CaMC^{69}W^{99}X^{145}$	0.11	0.09	1.2	0.08	⟨11⟩	4.1
	(0.01)	(0.01)	(0.1)	(0.01)		
			+Calcium			
$CaMC^{69}W^{99}$ [c]	0.24	0.06	1.1	0.22	⟨12⟩	1.2
	(0.01)	(0.02)	(0.3)	(0.02)		
$CaMC^{69}W^{99}X^{145}$	0.216	0.02	4	0.20	⟨12⟩	4.5
	(0.005)	(0.01)	(1)	(0.01)		

[a] Indicated values and associated standard errors of the mean (in parentheses) for three independent measurements were obtained from a two-exponential fit to frequency-domain data, essentially as described in the legend to Table 5. [b] Bracketed values were held fixed in the data analysis, as described in the text. [c] Data obtained from ref *7*. Experimental conditions are described in the legend of Figure 7.

Complementary measurements of the rotational dynamics of Trp^{99}, whose carbonyl group is expected to function as a calcium-binding ligand within calcium-binding site 3, permit an assessment of local structural changes within the carboxyl-terminal domain resulting from deletion of the four carboxyl-terminal amino acids. We have therefore measured the frequency response of Trp^{99} at 20 frequencies between 5 and 250 MHz for $CaMC^{69}W^{99}X^{145}$ (data not shown). An adequate fit to the data requires two rotational correlation times, associated with the segmental rotational dynamics of Trp (ϕ_1) and the global rotational motion of CaM (ϕ_2) (Table 6). Because of the short excited-state lifetime of Trp ($\langle\tau\rangle \sim 2-4$ ns), the value of the longer rotational correlation time is poorly determined. Therefore, in the determination of the rotational dynamics of Trp we have assumed the value for ϕ_2 measured using AEDANS bound to Cys^{69} (Table 5). We find that the segmental rotational dynamics of Trp^{99} are very similar in apo-CaM for $CaMC^{69}W^{99}$ and $CaMC^{69}W^{99}X^{145}$ (Table 6). However, upon calcium activation the segmental rotational dynamics of Trp^{99} in $CaMC^{69}W^{99}X^{145}$ becomes much slower than that observed in $CaMC^{69}W^{99}$, indicating that the environment around Trp^{99} becomes motionally restricted. These latter results are consistent with the large decrease in the solvent accessibility of Trp^{99} upon calcium activation in $CaMC^{69}W^{99}X^{145}$ compared with $CaMC^{69}W^{99}$ (Figure 8, Table 3). Thus, in conjunction with other data (see above), these results suggest that calcium binding results in a collapsed structure in which additional steric restraints result from structural interactions between the opposing domains that function to restrict the rotational dynamics of Trp^{99} in $CaMC^{69}W^{99}X^{145}$.

DISCUSSION

Summary of Results. We have expressed and purified a CaM mutant ($CaMC^{69}W^{99}X^{145}$) deficient in the carboxyl-terminal four amino acids between Met^{145} and Lys^{148}, allowing the investigation of the structural linkage between the carboxyl-terminal sequence and other secondary and tertiary structural elements within CaM. Deletion of the four carboxyl-terminal amino acids results in the loss of one high-affinity calcium-binding site and a large decrease in secondary structure (Figure 5), bringing the opposing globular domain of $CaMC^{69}W^{99}X^{145}$ into closer proximity following calcium activation (Figure 10, Table 4). The conformational heterogeneity observed between the opposing domains in

$CaMC^{69}W^{99}X^{145}$ is comparable to that of $CaMC^{69}W^{99}$, as evidenced by the narrow half-width of the Gaussian distance distribution (Figure 10). In addition, the rotational dynamics of the opposing globular domains remain structurally coupled, and there is a 3-fold reduction in the solvent accessibility of Trp^{99} in calcium-activated $CaMC^{69}W^{99}X^{145}$ compared with full-length $CaMC^{69}W^{99}$ (Tables 3−5; Figures 9 and 11). Thus, deletion of Met^{145}-Lys^{148} results in the formation of a new and stable conformation that probably involves direct contact interactions between the opposing globular domains. $CaMC^{69}W^{99}X^{145}$ is able to fully activate the PM−Ca−ATPase, albeit with a reduced apparent affinity (Figure 4). Thus, in the presence of the PM−Ca−ATPase $CaMC^{69}W^{99}X^{145}$ is able to assume the normal conformation necessary for enzyme activation, consistent with earlier examples in which the conformation of structurally modified CaM mutants have been shown to adopt native-like structures upon binding to target proteins (*32*−*34*). The reduction in the binding affinity between $CaMC^{69}W^{99}X^{145}$ and the PM−Ca−ATPase is consistent with the loss of specific binding interactions or, alternatively, may be the result of competition between binding interactions involving the opposing globular domains in $CaMC^{69}W^{99}X^{145}$ and the CaM-binding sequence of the PM−Ca−ATPase.

Relationships to Previous Studies. The opposing domains in calcium-activated CaM are connected by a metastable α-helical structure that is disrupted upon binding to target peptides (*2*, *7*, *10*−*13*, *29*, *58*, *69*, *70*). The flexibility of the central helix has been suggested to enable the amino- and carboxyl-terminal domains of CaM to recognize variable binding sequences in target proteins (*71*, *72*). Oxidative modification of a carboxyl-terminal methionine (Met^{144} or Met^{145}) or deletion of the carboxyl-terminal four amino acids (Figure 4) alters the structure of the central helix (*25*, *26*, *28*). These results suggest that the carboxyl-terminal sequence plays a structural role in maintaining the spatial separation between the opposing domains so as to either prevent the formation of stable interdomain interactions or restrict the relative positions and orientation of the two domains in CaM for optimal target recognition. Consistent with this suggestion, a direct structural coupling between the opposing globular domains of CaM are mediated by the structural features associated with calcium-binding site 4 located near the carboxyl terminus (*9*, *18*, *19*, *63*, *64*). Likewise, enhanced interactions between the opposing globular domains of calcium-binding site mutants of *Drosophila* CaM have been observed, where mutations in calcium-binding site 4 have the most deleterious structural consequences and result in the most substantial functional effects with respect to the activation of different CaM-dependent target enzymes, including the PM−Ca−ATPase (*21*, *24*). Thus, primary sequence differences within calcium-binding site 4 that are associated with the loss of high-affinity calcium binding results in a more compact tertiary structure that brings the opposing domains into closer proximity. Similar structural interactions are observed between the opposing globular domains in $CaMC^{69}W^{99}X^{145}$, which also correlate with the loss of one high-affinity calcium-binding site. Taken together, these results suggest that occupancy of both calcium-binding sites in the carboxyl-terminal domain are necessary to maintain CaM in an extended conformation following calcium activation.

However, while CaM isolated from *Saccharomyces cerevisiae* deficient in calcium-binding site 4 poorly activates CaM-dependent enzymes from vertebrates and mutations in calcium-binding site 4 that block calcium binding (i.e., $Glu^{140} \rightarrow Gln^{140}$ or Lys^{140}) in *Drosophila* CaM have previously been shown to result in an inability to activate the PM−Ca−ATPase (*22*−*24*), $CaMC^{69}W^{99}X^{145}$ can fully activate the PM−Ca−ATPase (Figure 4). This result can be understood by the fact that binding to target proteins can restore calcium binding for some calcium site mutations (i.e., $Gln^{140}Ala^{140}$), consistent with the ability of this latter CaM mutant to fully activate the PM−Ca−ATPase (*32*, *33*). This latter observation is furthermore consistent with previous reports in which the structure and function of conformationally altered CaM molecules resulting from elimination of any of the four calcium-binding ligands are restored to varying extents upon binding to peptides corresponding to the CaM-binding sequence of skeletal myosin light chain kinase. Furthermore, there is a correlation between the ability of target peptides to restore native-like structure with the functional activation of skeletal myosin light chain kinase by these mutant CaM's (*20*, *34*). Therefore, since $CaMC^{69}W^{99}X^{145}$ retains the ligands associated with calcium binding in site 4, the ability to fully activate the PM−Ca−ATPase suggests that $CaMC^{69}W^{99}X^{145}$ binding to the PM−Ca−ATPase promotes the productive interactions necessary to restore the native-like structure necessary for function and to restore calcium binding.

Conclusions and Future Directions. We have identified a structural linkage between the four amino acids at the carboxyl terminal and the opposing globular domains of CaM, which are critical in maintaining calcium-activated CaM in an extended conformation. Enhanced interaction between the opposing globular domains in $CaMC^{69}W^{99}X^{145}$ does not impair the ability to fully activate the PM−Ca−ATPase under equilibrium conditions, emphasizing that alterations in the average conformation of the central helix are not critical to function. However, the reduced affinity between $CaMC^{69}W^{99}X^{145}$ and the PM−Ca−ATPase does suggest that the maintenance of CaM in an extended conformation may function to minimize structural interactions between the opposing domains and facilitate high-affinity binding to the PM−Ca−ATPase. These results suggest that the native conformation of the carboxyl-terminal domain may be necessary for the rapid association of CaM with a range of different target proteins necessary for rapid intracellular signaling. Future studies should be directed at identifying specific structural interactions that are important in the stabilization of the central helix and their possible role in mediating the rapid collapse of CaM around a range of different target proteins.

ACKNOWLEDGMENT

We thank Michail Alterman and Sara Mounter for their help in DNA sequencing, Professor Robert F. Weaver and Judy L. Bevan for helpful advice involving molecular cloning and site-directed mutagenesis, and Dr. Todd D. Williams for mass spectrometry measurements.

REFERENCES

1. James, P., Vorherr, T., and Carafoli, E. (1995) *Trends Biochem. Sci. 20*, 38−42.
2. Babu, Y. S., Bugg, C. E., and Cook, W. J. (1988) *J. Mol. Biol. 204*, 191−204.

3. LaPorte, D. C., Wierman, B. M., and Storm, D. R. (1980) *Biochemistry 19*, 3814−3819.
4. Krebs, J., Buerkler, J., Guerini, D., Brunner, J., and Carafoli, E. (1984) *Biochemistry 23*, 400−403.
5. Nelson, M. R., and Chazin, W. J. (1998) *Protein Sci. 7*, 270−282.
6. Sorensen, B. R., and Shea, M. A. (1996) *Biophys. J. 71*, 3407−3420.
7. Sun, H., Yin, D., and Squier, T. C. (1999) *Biochemistry 38*, 12266−12279.
8. Pedigo, S., and Shea, M. A. (1995) *Biochemistry 34*, 1179−1196.
9. Sorensen, B. R., and Shea, M. A. (1998) *Biochemistry 37*, 4244−4253.
10. Ikura, M., Clore, G. M., Gronenborn, A. M., Zhu, G., Klee, C. B., and Bax, A. (1992) *Science 256*, 632−638.
11. Meador, W. E., Means, A. R., and Quiocho, F. A. (1992) *Science 257*, 1251−1255.
12. Meador, W. E., Means, A. R., and Quiocho, F. A. (1993) *Science 262*, 1718−1721.
13. Barbato, G., Ikura, M., Kay, L. E., Pastor, R. W., and Bax, A. (1992) *Biochemistry 31*, 5269−5278.
14. Ikura, M., Spera, S., Barbato, G., Kay, L. E., Krinks, M., and Bax, A. (1991) *Biochemistry 30*, 9216−9228.
15. Persechini, A., McMillan, K., and Leakey, P. (1994) *J. Biol. Chem. 269*, 16148−16154.
16. Bayley, P. M., Findlay, W. A., and Martin, S. R. (1996) *Protein Sci. 5*, 1215−1228.
17. Barth, A., Martin, S. R., and Bayley, P. M. (1998) *J. Biol. Chem. 273*, 2174−2183.
18. Starovasnik, M. A., Davis, T. N., and Klevit, R. E. (1993) *Biochemistry 32*, 3261−3270.
19. Nakashima, K., Ishida, H., Ohki, S., Hikichi, K., and Yazawa, M. (1999) *Biochemistry 38*, 98−104.
20. Martin, S. R., Maune, J. F., Beckingham, K., and Bayley, P. M. (1992) *Eur. J. Biochem. 205*, 1107−1114.
21. Maune, J. F., Beckingham, K., Martin, S. R., and Bayley, P. M. (1992) *Biochemistry 31*, 7779−7786.
22. Luan, Y., Matsuura, I., Yazawa, M., Nakamura, T., and Yagi, K. (1987) *J. Biochem. 102*, 1531−1537.
23. Ohya, Y., Uno, I., Ishikawa, T., and Anraku, Y. (1987) *Eur. J. Biochem. 168*, 13−19.
24. Gao, Z. H., Krebs, J., VanBerkum, M. F. A., Tang, W., Maune, J. F., Means, A. R., Stull, J. T., and Beckingham, K. (1993) *J. Biol. Chem. 268*, 20096−20104.
25. Yao, Y., Yin, D., Jas, G. S., Kuczer, K., Williams, T. D., Schöneich, C., and Squier, T. C. (1996) *Biochemistry 35*, 2767−2787.
26. Gao, J., Yin, D. H., Yao, Y., Sun, H., Qin, Z., Schöneich, C., Williams, T. D., and Squier, T. C. (1998) *Biophys. J. 74*, 1115−1134.
27. Gao, J., Yao, Y., Yin, D., Williams, T. D., and Squier, T. C. (1998) *Biochemistry 37*, 9536−9548.
28. Yin, D., Kuczera, K., and Squier, T. C. (2000) *Chem. Res. Toxicol. 13*, 103−110.
29. Chattopadhyaya, R., Meador, W. E., Means, A. R., and Quiocho, F. A. (1992) *J. Mol. Biol. 228*, 1177−1192.
30. Yin, D., Sun, H., Weaver, R. F., and Squier, T. C. (1999) *Biochemistry 38*, 13654−13660.
31. Mukherjea, P., Maune, J. F., and Beckingham, K. (1996) *Protein Sci. 5*, 468−477.
32. Haiech, J., Kilhoffer, M.-C., Lukas, T. J., Craig, T. A., Roberts, D. M., and Watterson, D. M. (1991) *J. Biol. Chem. 266*, 3427−3431.
33. Bzedga, T., and Kosk-Kosicka, D. (1992) *J. Biol. Chem. 267*, 4394−4397.
34. Findlay, W. A., Martin, S. R., Beckingham, K., and Bayley, P. M. (1995) *Biochemistry 34*, 2087−2094.
35. Strasburg, G. M., Hogan, M., Birmachu, W., Thomas, D. D., and Louis, C. F. (1988) *J. Biol. Chem. 263*, 542−548.
36. Hühmer, A. F., Gerber, N. C., de Montellano, P. R., and Schöneich, C. (1996) *Chem. Res. Toxicol. 9*, 484−491.
37. Niggli, V., Penniston, J. T., and Carafoli, E. (1979) *J. Biol. Chem. 254*, 9955−9958.
38. Gornal, A. G. (1949) *J. Biol. Chem. 177*, 751−766.
39. Lanzetta, P. A., Alvarez, L. J., Reinach, P. S., and Candia, O. A. (1979) *Anal. Biochem. 100*, 95−97.
40. Fabiato, A. (1988) *Methods Enzymol. 157*, 378−417.
41. Persechini, A., McMillan, K., and Leakey, P. (1994) *J. Biol. Chem. 269*, 16148−16154.
42. Sun, H., and Squier, T. C. (2000) *J. Biol. Chem.* 275, 1731−1738.
43. Venyaminov, S. Y., and Yang, J. T. (1996) in *Circular Dichroism and the Conformational Analysis of Biomolecules* (Fasman, G. D., Ed.), pp 69−107, Plenum Press, New York.
44. Haas, E., Katchalski-Katzir, E., and Steinberg, I. Z. (1978) *Biochemistry 17*, 5064−5070.
45. Lakowicz, J. R., Gryczynski, I., Cheung, H. C., Wang, C., Johnson, M. L., and Joshi, N. (1988) *Biochemistry 27*, 9149−9160.
46. Wu, P., and Brand, L. (1992) *Biochemistry 31*, 7939−7947.
47. Klee, C. B., Crouch, T. H., and Krinks, M. H. (1979) *Proc. Natl. Acad. Sci. U.S.A. 76*, 6270−6273.
48. Zhang, M., Li, M., Wang, J. H., and Vogel, H. J. (1994) *J. Biol. Chem. 269*, 15546−15552.
49. Carafoli, E. (1987) *Annu. Rev. Biochem. 56*, 395−433.
50. Finn, B. E., Evenas, J., Drakenberg, T., Waltho, J. P., Thulin, E., and Forsen, S. (1995) *Nat. Struct. Biol. 2*, 777−783.
51. Kuboniwa, H., Tjandra, N., Grzesiek, S., Ren, H., Klee, C. B., and Bax, A. (1995) *Nat. Struct. Biol. 2*, 768−776.
52. Urbauer, J. L., Short, J. H., Dow, K. W., and Wand, A. J. (1995) *Biochemistry 34*, 8099−8109.
53. Zhang, M., Tanaka, T., and Ikura, M. (1995) *Nat. Struct. Biol. 2*, 758−767.
54. Beckingham, K. (1991) *J. Biol. Chem. 266*, 6027−6030.
55. Seamon, K. B. (1980) *Biochemistry 19*, 207−215.
56. Klevit, R. E., Dalgarno, D. C., Levine, B. A., and Williams, R. J. P. (1984) *Eur. J. Biochem. 139*, 109−114.
57. Kilhoffer, M.-C., Roberts, D. M., Adibi, A. O., Watterson, D. M., and Haiech, J. (1988) *J. Biol. Chem. 263*, 17023−17029.
58. Yao, Y., Schöneich, C., and Squier, T. C. (1994) *Biochemistry 33*, 7797−7810.
59. Linse, S., Helmersson, A., and Forsen, S. (1991) *J. Biol. Chem.* 266, 8050−8054.
60. Willis, K. J., Neugebauer, W., Sikorska, M., and Szabo, A. G. (1994) *Biophys. J. 66*, 1623−1630.
61. Dahms, T. E. S., and Szabo, A. G. (1995) *Biophys. J. 69*, 569−576.
62. Kuboniwa, H., Tjandra, N., Grzesiek, S., Ren, H., Klee, C. B., and Bax, A. (1995) *Nat. Struct. Biol. 2*, 768−776.
63. Yoshino, H., Izumi, Y., Sakai, K., Takezawa, H., Matsuura, I., Maekawa, H., and Yazawa, M. (1996) *Biochemistry 35*, 2388−2393.
64. Lee, S. Y., and Klevit, R. E. (2000) *Biochemistry* 39, 4225−4230.
65. Cheung, H. C. (1991) in *Topics in Fluorescence Spectroscopy* (Lakowicz, J. R., Ed.) pp 128−176, Plenum Press, New York.
66. Tjandra, N., Bax, A., Crivici, A., and Ikura, M. (1999) in *Calcium as a Cellular Regulator* (Carafoli, E., and Klee, C., Eds), pp 152−170, Oxford University Press, Oxford.
67. Small, E. W., and Anderson, S. R. (1988) *Biochemistry 27*, 419−428.
68. Török, K., Lane, A. N., Martin, S. R., Janot, J.-M., and Bayley, P. M. (1992) *Biochemistry 31*, 3452−3462.
69. Spera, S., Ikura, M., and Bax, A. (1991) *J. Biomol. NMR 1*, 155−165.
70. Clore, G. M., Bax, A., Ikura, M., and Gronenborn, A. M. (1993) *Curr. Opin. Struct. Biol. 3*, 838−845.
71. Vogel, H. J. (1994) *Biochem. Cell Biol. 72*, 357−376.
72. van der Spoel, D., Vogel, H. J., and Berendsen, H. J. (1996) *Proteins 24*, 450−466.
73. Kawasaki, H., and Kretsinger, R. (1995) *Protein Profile 2*, 334−335.
74. Eftink, M. R., and Ghiron, C. A. (1976) *Biochemistry 15*, 672−680.
75. Kraulis, P. J. (1991) *J. Appl. Crystallogr. 24*, 946−950.
76. Laemmli, U. K. (1970) *Nature 227*, 680−685.

BI000949Y